Diamond & Related Materials 146 (2024) 111195

Contents lists available at ScienceDirect

Diamond & Related Materials

journal homepage: www.elsevier.com/locate/diamond

Investigation of drug delivery capability of single-walled carbon and boron-nitride nanotubes, boron-nitride ($B_{16}N_{16}$), and C_{32} fullerenes as nanocarriers of captopril drug; DFT study

Khourshid Mehdizadeh [a,*], Farzad Toiserkani [b], Mohammad Javad Khodabakhshi [c], Narjes Hajali [c], Majid Farsadrooh [d,*]

[a] Department of Chemistry, Roudsar and Amlash Branch, Islamic Azad University, Roudsar, Iran
[b] Schoool of Polymer Science and Polymer Engineering, The University of Akron, Akron, OH 44325, United States
[c] Department of Chemistry, Islamic Azad University, Central Tehran Branch, Tehran, Iran
[d] Renewable Energies Research Laboratory, Department of Chemistry, Faculty of Science, University of Sistan and Baluchestan, P.O. Box 98135 674, Zahedan, Iran

ARTICLE INFO

Keywords:
$B_{16}N_{16}$ fullerene
Boron nitride
Captopril
C_{32} fullerene
Drug delivery
Nanosensor

ABSTRACT

Density functional theory (DFT) calculations were performed on M062X/6-31G (d) and M062X/6-311G (d, p) surfaces to investigate the interaction of captopril molecules with single-walled carbon nanotubes (SWCNT) and C_{32} nanoclusters. In order to enhance adsorption, a doping method was employed, and structures of single-walled boron nitride nanotubes (SWBNNT) and boron nitride nanoclusters ($B_{16}N_{16}$) were selected for improved drug delivery purposes in this study. The adsorption energy of captopril on the nanostructures was calculated in both phases. In both phases, captopril adsorption energy on nanostructures was calculated. The negative values of adsorption energy showed that the interaction between captopril and nanostructures is exothermic. The adsorption energy values were higher in the gas phase compared to the aqueous phase, indicating a stronger interaction in the gas phase. The density of states (DOS) study was employed to evaluate the effect of molecular adsorption on the electronic properties of nanostructures. The results revealed that the $B_{16}N_{16}$ nanocluster approached the Fermi level more closely after drug adsorption compared to other nanostructures. Quantum Theory of Atoms in Molecules (QTAIM) calculations showed that there is a weak interaction between captopril and both nanostructures. Based on the adsorption energy values obtained from both methods, the interaction between captopril and SWCNT was found to be stronger than that between captopril and SWBNNT, whereas the interaction in the $B_{16}N_{16}$ nanocluster was found to be equal to that in C_{32}-fullerene. Significant changes in ΔE_g values were observed for Captopril@SWCNT and Captopril@$B_{16}N_{16}$-fullerene in each method, indicating the conductivity of these two structures increased more after captopril adsorption compared to other nanostructures. Therefore, SWBNNT and $B_{16}N_{16}$-fullerene can serve as captopril nanosensors.

1. Introduction

Since blood pressure typically elevates with age, the prevalence of hypertension and the administration of high-dosage antihypertensive medicines for its management have been predicted to increase with growing life expectancy [1]. Captopril is an orally active inhibitor of angiotensin-converting enzyme (the enzyme responsible for the conversion of angiotensin I to angiotensin II) belonging to the sulfhydryl group that prevents (blocks) the converting enzyme in the body from making angiotensin II, leading to reducing peripheral resistance and relaxation of blood vessels and finally reducing blood pressure [2–4]. It is well known that captopril is prescribed to decrease rheumatoid arthritis symptoms, treatment of congestive heart failure, Raynaud's phenomenon, angina, and safeguard kidney function in diabetic nephropathy [2,5,6]. However, when this medicine is taken orally, its therapeutic action lasts 6–8 h because it has a 1.7–2.0 h elimination half-life, hence the clinically recommended daily dose is 37.5–75 mg administered three times per day. Previous research indicates that the oxidation rate of captopril in dermal homogenates is significantly lower than that in intestinal homogenates because captopril disulfide, which

* Corresponding authors.
E-mail addresses: mehdizadeh.2030@gmail.com (K. Mehdizadeh), farsadroohmajid@gmail.com (M. Farsadrooh).

https://doi.org/10.1016/j.diamond.2024.111195
Received 5 January 2024; Received in revised form 5 May 2024; Accepted 11 May 2024
Available online 13 May 2024
0925-9635/© 2024 Elsevier B.V. All rights are reserved, including those for text and data mining, AI training, and similar technologies.

derives from the oxidation of captopril, is difficult to absorb from the intestine. Hence, the development of a controlled delivery system for captopril would bring numerous benefits to patients. Previous research indicates that the oxidation rate of captopril in dermal homogenates is significantly lower than that in intestinal homogenates because captopril disulfide, which derives from the oxidation of captopril, is difficult to absorb from the intestine. Hence, the development of a controlled delivery system for captopril would bring numerous benefits to patients.

Typically, nanocarriers are characterized as nano-scale systems used to convey biologically active cargo, like pharmaceuticals [7,8]. The utilization of nanostructures for the targeted transfer of drugs causes to reduces the toxicity of the drug and improves therapeutic efficiency. Nanostructures, due to their dimensions, can effectively cross biological and physiological barriers, hence, when the size of drug carriers reduces to nano dimensions provides numerous advantages, including improved pharmacokinetic profiles and enhanced biodistribution of therapeutic agents, thanks to the large aspect ratio [9]. Various carbon allotropes, such as graphene, fullerene, and carbon nanotubes have been utilized in different biological applications, like drug delivery, cell targeting, and bioimaging [10]. Single-walled carbon nanotubes (SWCNTs) are highly significant and extensively utilized materials that have gained popularity among scientists, especially in the field of drug delivery systems [11,12]. This is primarily due to their exceptional properties, including stability, strength, and reservoir-like structure, which enable spontaneous storage and protection of active drug molecules from degradation [11]. Novel drug delivery systems based on SWCNTs have been used to treat a variety of diseases due to their size, increased stability, strong biocompatibility, large surface area, and high drug-loading capacity. The deep potential well inside the CNT allows for easy encapsulation of molecules, making it a unique system for various types of molecular transport, particularly biomolecules and drug cargoes [9].

Recently, boron nitride nanomaterials have received a great deal of attention from researchers on account of their unique structure and properties. Boron nitride nanotubes (BNNTs) are structural analogs of carbon nanotubes (CNTs), in which nitrogen and boron atoms alternately replace carbon atoms in a resonance hybrid that presents high thermal stability and good chemical inertia [13,14]. BNNTs are promising alternative nanocarriers providing several advantages, including a large inner volume for encapsulating more drugs, various inner and outer surfaces, and generally open ends that allow the drug to penetrate if the energy interaction is favorable [15]. In addition, numerous other studies emphasize the biosafety of BNNTs and show that they are biocompatible [16] without causing oxidative DNA damage or apoptosis [17]. The charge distribution of BNNTs is asymmetric in B—N bonds, and the electron density of B is adsorbed to the N atoms on account of nitrogen's higher electronegativity.

Carbon fullerenes offer several advantages as drug carriers [18,19]. Unlike other nanoparticles, the size and shape of fullerenes are highly reproducible. Furthermore, fullerenes are non-toxic and biocompatible compounds. Like in other sp^2 hybridized systems, each fullerene carbon atom can make a covalent bond with the drug, which serves as a functional group linker molecule [20]. Fullerenes, on the other hand, can bind noncovalently with the aromatic rings of the drug molecule via π-π coupling [20]. Similar to different carbon allotrope structures, nitride, and boron can be present in structures of fullerene ranging in size from 0.7 to 1.4 nm. The general morphology of boron nitride fullerenes is typically composed of even-membered rings, with six tetragons replacing the 12 pentagons in the carbon fullerenes formula to entirely eliminate homoelemental links [21]. Boron nitride materials are chemically stable [22], mainly owing to the ionic bond created between negatively charged N atoms and positively charged B atoms [23]. In these structures, the N atoms prefer to hybridize with the B atom in sp^3, resulting in a local pyramidal structure. In terms of structural stability, $B_{12}N_{12}$ fullerene, which consists of six tetragon rings and eight hexagon rings, is regarded as the most stable fullerene among its counterparts. Because of the ionic nature of chemical bonds and the local pyramidal structures, such structures possess a strong inclination to bind with other molecules, either chemically or physically. Investigation of the interaction of aspirin, hydrogen halides, H_2S gas, metformin, pyrimidine nucleotide, phenol molecule, 5-fluorouracil, 5-aminolevulinic acid, cytosine, uracil, adenine, cysteine, nicotine and caffeine with the $B_{12}N_{12}$ fullerene and its derivatives utilizing computational approaches have been performed in previous literature [23]. This evidence demonstrates that the nanocage cluster has a high potential to create interaction with biological molecules, making it a promising material for biomedical applications, such as biosensing, bioimaging, and drug delivery.

In this work, the captopril drug was selectively loaded on a single-walled boron nitride nanotube (SWBNNT), single-walled carbon nanotube (SWCNT), C_{32} and $B_{16}N_{16}$ fullerenes. Computations of the quantum theory of atoms in molecules (QTAIM) were employed for these systems to determine the nature of interactions and bonds between nanostructures (SWCNT and SWBNNT) and captopril. Calculations of Density functional theory (DFT) were also carried out to examine the possibility of applying SWCNT SWBNNT, C_{32}, and $B_{16}N_{16}$ fullerenes nanostructures as captopril drug delivery systems.

2. Computational methods

In this study, carbon (6,0) zigzag nanotubes, boron nitride (6,0) zigzag nanotubes, C_{32} and $B_{16}N_{16}$ fullerenes are investigated for delivering captopril drug. Calculations of DFT were accomplished utilizing the M062X method, the 6-31G (d) and 6-311G (d, p) basis set, and the GAMESS-US software [24–28]. The goal was to gain the levels of molecular electrostatic potential (MEP), the results of the density of states (DOS), the natural bond orbital (NBO) analysis [29–32], and determine the type of drug and nanostructures interaction using the calculations of the quantum theory of atoms in molecules (QTAIM) [33,34]. All DFT calculations were performed on the compounds' ground state. In addition, the charge and spin of the compounds were selected as 0 and 1 (singlet), respectively. To model nanotubes and interact with the structures, Nanotube Modeler [35], graphical software, and Gauss View 5.0, were applied. The density of state (DOS) diagrams were plotted with GaussSum v3.0 software [36]. The results were evaluated by Chemcraft software. In order to calculate the adsorption energy (E_{ads}) of captopril molecules at the level of nanostructures, the following equation was used [37]:

$$E_{ads} = \left(E_{complex}\right) - \left(E_{nanostructure} + E_{captopril}\right) \quad (1)$$

$E_{captopril}$ and $E_{nanostructure}$ are the values of primary energy of captopril and nanostructures, respectively. $E_{complex}$ is the total energy of nanostructures and captopril; The negative value of adsorption energy indicates that the process is exothermic. QTAIM calculations were accomplished to assess the properties of bond critical points. To examine the optimized complexes and kinds of molecules and atoms involved in the interaction, the AIM2000 program was used. Chemical properties and different kinds of interactions and bonds can be precisely determined using QTAIM calculations. This method was used for atom-atom interactions, intermolecular interactions, determining bond critical points, charge density $(\rho(r))$, and the Laplacian of the charge density $(\nabla^2\rho(r))$. The counterpoise method was utilized to correct the basis set superposition error (BSSE) for the adsorption energy.

3. Results and discussion

3.1. Captopril adsorption onto SWCNT

The SWCNT under study was a (6, 0) zigzag nanotube with a length of 13.55 Å and a diameter of 4.69 Å. The optimized geometric shape nanostructure of SWCNT has two kinds of C—C bonds of different lengths. An axial bond with a length of 1.41 Å and a diagonal bond with a length of 1.43 Å. The investigated SWCNT was comprised of 72 C and

12 H atoms. Optimal structures of the captopril molecule, SWCNT, SWBNNT, and C_{32} and $B_{16}N_{16}$ fullerene nanostructures are shown in Fig. 1. The captopril molecule was first placed in various positions on the external surface of the SWCNT with various orientations. Fig. 2 shows the best and most stable position of the captopril on the SWCNT surface. Table 1 demonstrates the computed values of the adsorption energy (E_{ads}), energy gap (E_g), and the difference between the adsorbed captopril onto nanostructure energy gap and nanostructure energy gap before adsorption of captopril (ΔE_g). The transferred charge (Q_T), which was gained following the Natural bond orbital (NBO) analysis, was positive; it indicates the charge transfer from captopril to SWCNT. The energy gap value (E_g) in SWCNT after adsorption decreased only slightly compared to before adsorption, indicating insignificant changes in conductivity. The E_{ads} values in both the gas and aqueous phases indicate that the adsorption of the captopril onto SWCNT was chemical. The negative values of captopril adsorption energy in both gaseous and aqueous phases imply that captopril adsorption on SWCNT is exothermic. The adsorption energy values of captopril on SWCNT show that SWCNT can be proposed as a drug delivery system for captopril molecule.

3.2. Captopril adsorption onto SWBNNT

The SWBNNT under study was a (6, 0) zigzag nanotube with a length of 13.64 Å and a diameter of 4.78 Å. This nanotube was comprised of 36 B, 36 N, and 12H atoms. The optimal geometric shape of the SWBNNT nanostructure has two kinds of B—N bonds with various lengths. Also, there is an axial B—N bond and a diagonal bond with lengths of 1.44 Å and 1.45 Å, respectively. The captopril molecule was first placed in various positions on the external surface of the SWBNNT with various orientations. Fig. 2b shows the best and most stable position of captopril on the SWBNNT surface. The transferred charge (Q_T) that was obtained following the Natural bond orbital (NBO) analysis was negative (Table 1), indicating that captopril is an electron acceptor in the Captopril@SWBNNT structure. The value of the energy gap (E_g) decreased after adsorption. This decrease in E_g indicates an increase in the conductivity of SWBNNT. E_{ads} values in gas and aqueous phases indicate that the adsorption of captopril onto SWBNNT is weaker compared to SWCNT. The energy of captopril adsorption was negative in both the gas and aqueous phases, indicating that the adsorption of captopril onto SWBNNT is exothermic. The obtained values of captopril adsorption

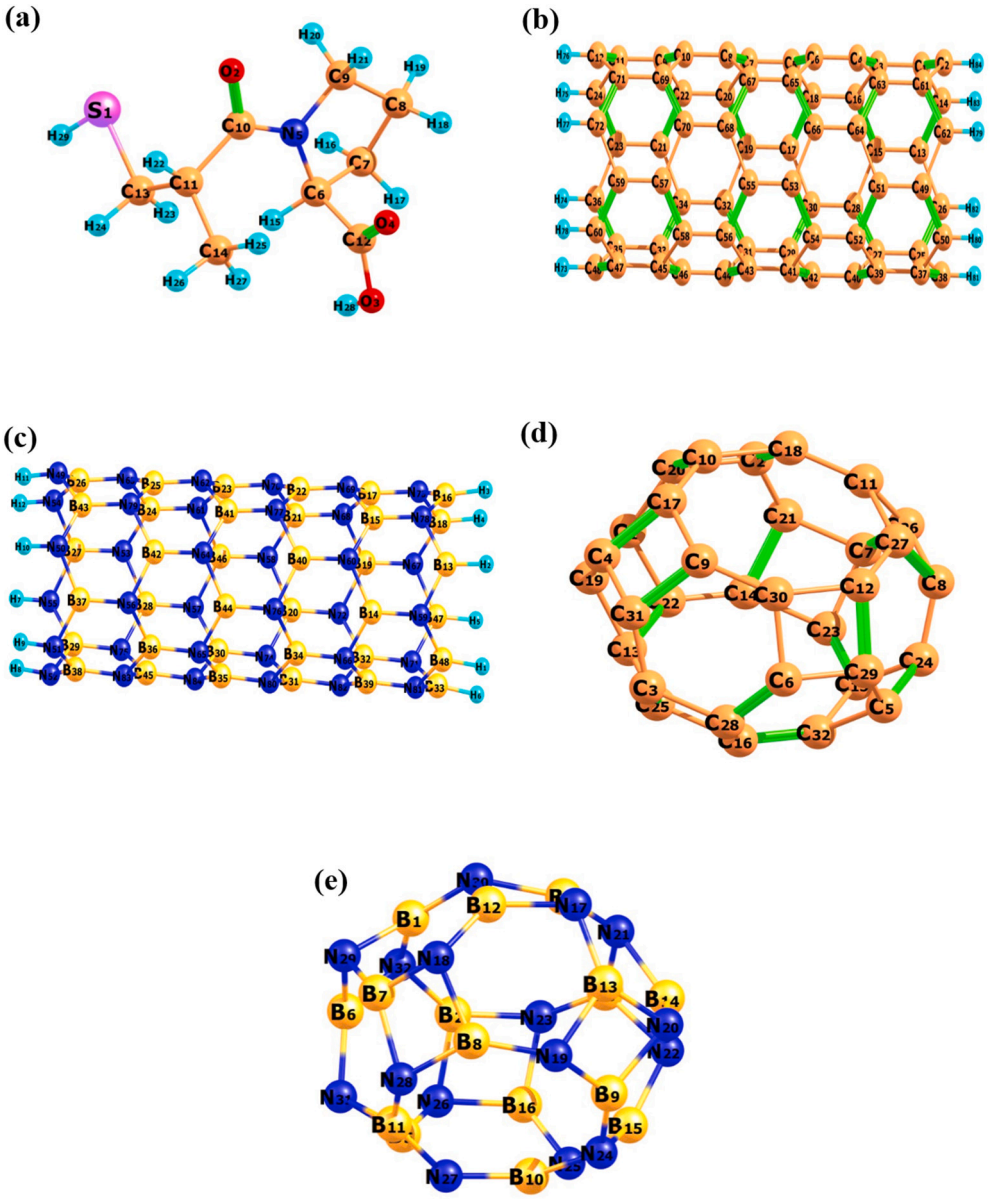

Fig. 1. Optimized structures of (a) captopril molecule, (b) SWCNT, (c) SWBNNT, (d) C_{32}-fullerene, and (e) $B_{16}N_{16}$-fullerene.

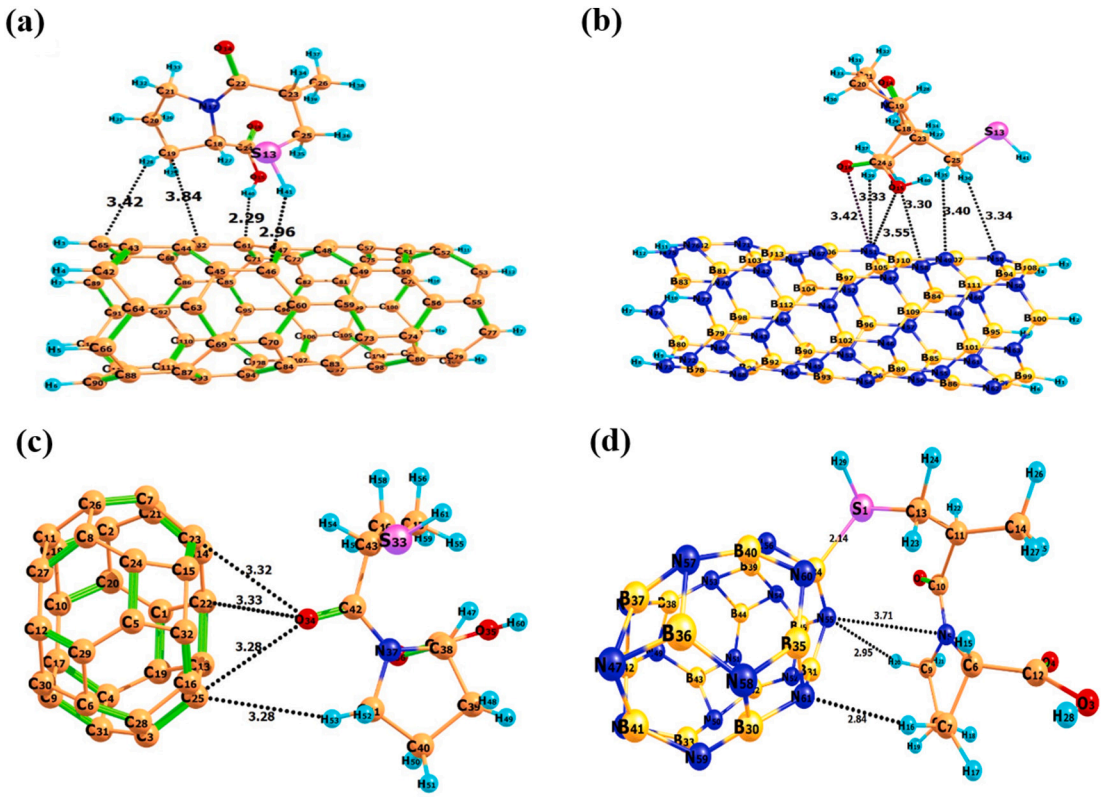

Fig. 2. Optimized structures of (a) Captopril@SWCNT, (b) Captopril@SWBNNT, (c) Captopril@C_{32}-fullerene, and (d) Captopril@$B_{16}N_{16}$-fullerene.

Table 1
The adsorption energy (E_{ads}) of captopril onto SWCNT, SWBNNT, C_{32}, and $B_{16}N_{16}$ fullerenes in aqueous and the gaseous phases, basis set superposition error (BSSE), charge transfer between captopril and nanostructures (Q_T), the HOMO-LUMO energy gaps (E_g) and the change of HOMO-LUMO gap energy upon the adsorption processes.

Nanostructures	HOMO (eV)	LUMO (eV)	E_{ads}(eV) in gas	E_{ads}(eV) in water	BSSE (eV)	E_g(eV)	ΔE_g(eV)	Q_T(e)
SWCNT	−3.9486	−2.3289	–	–	–	1.6196	–	–
SWBNNT	−8.1554	−1.1047	–	–	–	7.0507	–	–
C_{32}-fullurene	−6.8907	−3.2596	–	–	–	3.6311	–	–
$B_{16}N_{16}$-fullurene	−9.3138	−0.2092	–	–	–	9.1047	–	–
Captopril@SWCNT	−4.3399	−2.7225	−0.4557	−0.3307	0.019	1.6174	−0.0022	+0.077
Captopril@SWBNNT	−8.0455	−1.1112	−0.3701	−0.1998	0.0051	6.9343	−0.1164	−0.001
Captopril@C_{32}-fullerene	−6.5157	−2.8811	−0.2734	−0.1997	0.0046	3.6346	+0. 0035	+0.002
Captopril@$B_{16}N_{16}$-fullerene	−8.5103	+0.1924	−0.6482	−0.8795	0.061	8.7027	−0.4020	−0.002

energy on SWBNNT indicate that the interaction between captopril and SWBNNT falls within the range of physical adsorption. Hence, SWBNNT can be introduced as a drug recognition or carrier system for captopril.

3.3. Captopril adsorption onto C_{32} fullerene

The optimized geometric shape of the C_{32} fullerene has four types of bonds between carbon atoms. In hexagons, C—C bonds had lengths of 1.48 Å, 1.38 Å, and 1.45 Å, and in octagonals, C—C bonds had lengths of 1.52 Å and 1.38 Å. The investigated C_{32} fullerene was comprised of 32 carbon atoms. The captopril molecule was first placed in various positions on the external surface of the C_{32} fullerene with different orientations. Fig. 2 shows the best and most stable position of captopril on the C_{32} fullerene surface. Natural bond orbital (NBO) analysis showed that the transferred charge (Q_T) of C_{32} fullerene was positive. It indicates the charge transfer from captopril to C_{32} fullerene. The energy gap value (E_g) of C_{32}-fullerene increased after adsorption. Thus, due to its lack of chemical reactivity, the C_{32} fullerene can only be considered as a weak adsorbent for captopril.

3.4. Captopril adsorption onto $B_{16}N_{16}$ fullerene

The $B_{16}N_{16}$ fullerene under study was composed of 16 boron and 16 nitrogen atoms. The optimized geometric shape of the nanostructure of $B_{16}N_{16}$ has five types of B—N bonds of different lengths. In hexagons, B—N bonds had lengths of 1.46 Å, 1.43 Å, and 1.50 Å, and in octagonals, B—N bonds had lengths of 1.48 Å and 1.43 Å. The captopril molecule was first placed in different positions on the external surface of the $B_{16}N_{16}$ with different orientations. Fig. 2d shows the best and most stable position of the captopril on the $B_{16}N_{16}$ surface. After interaction with captopril, the HOMO energy level increased by 0.8035 eV. This indicates that $B_{16}N_{16}$ fullerene is an electron donor and captopril must also act as an electron acceptor. On the other hand, the boron atom with number 34, the nitrogen atom with number 55, and the nitrogen atom with number 61 in the $B_{16}N_{16}$ fullerene interact with the sulfur atom, the nitrogen atom with number 5, and the hydrogen atoms with numbers 20 and 16 of captopril, respectively. Electron transfer is more easier in $B_{16}N_{16}$ fullerene compared to C_{32} fullerene. Therefore, the adsorption energy of $B_{16}N_{16}$ fullerene is much higher than C_{32} fullerene.

The transferred charge (Q_T), which was gained following the Natural bond orbital (NBO) analysis, was negative (Table 1); it indicates that captopril is an electron acceptor in the Captopril@$B_{16}N_{16}$ structure. The value of the energy gap (E_g) significantly decreased after adsorption. E_{ads} values in gaseous and aqueous phases show that captopril forms a stronger bond with $B_{16}N_{16}$ than with SWBNNT, SWCNT, and C_{32}. Adsorption energies of captopril in both the gas and aqueous phases were negative, indicating that captopril adsorption on $B_{16}N_{16}$ is exothermic. Captopril adsorption energy values on $B_{16}N_{16}$ show that the interaction of captopril with $B_{16}N_{16}$ is chemical adsorption, subsequently leading to a significant increase in the conductivity of $B_{16}N_{16}$. Therefore, $B_{16}N_{16}$ can be introduced as a recognition system for

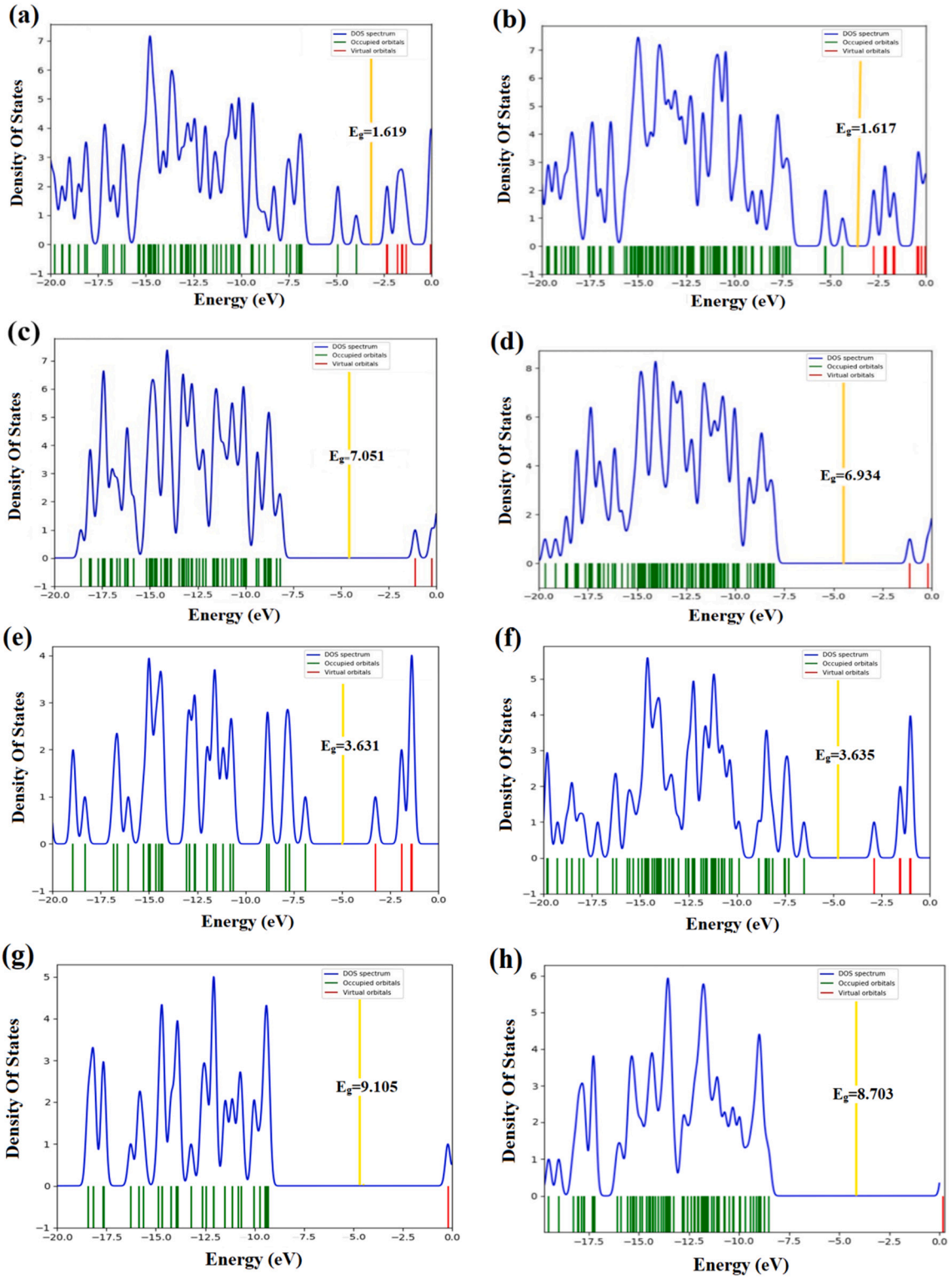

Fig. 3. (a) DOS spectra for SWCNT, (b) DOS spectra for Captopril@SWCNT, (c) DOS spectra for SWBNNT, (d) DOS spectra for Captopril@SWBNNT, (e) DOS spectra for C_{32}-fullerene, (f) DOS spectra for Captopril@C_{32}-fullerene, (g) DOS spectra for $B_{16}N_{16}$-fullerene and DOS spectra for Captopril@$B_{16}N_{16}$-fullerene (h). The yellow indicates the Fermi level. (For interpretation of the references to colour in this figure legend, the reader is referred to the web version of this article.)

captopril molecule in drug delivery.

3.5. Density of states (DOS)

The density of states (DOS) was determined in order to explore the impact of surface adsorption of the captopril molecule on the electronic characteristics of nanostructures. The density of states diagrams of SWCNT, Captopril@SWCNT, SWBNNT, Captopril@SWBNNT, C_{32}-fullerene, Captopril@C_{32}-fullerene, $B_{16}N_{16}$-fullerene, and Captopril@$B_{16}N_{16}$-fullerene are shown in Fig. 3 (a-h). After the interaction of nanostructures with captopril, results showed that the HOMO and LUMO energy levels of the SWBNNT and $B_{16}N_{16}$ fullerene got closer to the Fermi energy level (the yellow line) compared to other nanostructures. In optimized conditions, the ΔE_g values for captopril adsorption onto SWBNNT, SWCNT, C_{32}-fullerene, and $B_{16}N_{16}$-fullerene were -0.1164 eV, −0.002 eV, +0.0035 eV, and -0.4020 eV, respectively. As demonstrated in DOS diagrams, the adsorption of captopril molecules onto SWBNNT leads to a change in the energy gap. Based on DOS analysis (Table 1), in Captopril@SWBNNT, and Captopril@$B_{16}N_{16}$-fullerene, the conduction and valence levels of molecular orbitals, respectively, were closer to higher and lower energy levels. As a result, the value of the SWBNNT and $B_{16}N_{16}$-fullerene energy gap decreased more than that of SWCNT and C_{32}-fullerene. Moreover, $B_{16}N_{16}$-fullerene's valence level in Captopril@$B_{16}N_{16}$-fullerene was closer to the Fermi level in comparison to SWCNT. Therefore, the conductivity of $B_{16}N_{16}$-fullerene after the interaction increased more than that of other nanostructures. The electrical conductivity (σ) of the molecular complexes at a given temperature can be determined by the following equation [12]:

$$\sigma \propto exp\left(\frac{-E_g}{KT}\right) \tag{2}$$

Here, σ represents electrical conductivity. K and T are the Boltzmann constant and temperature. Based on Eq. (2), if the value of E_g at a hypothetical temperature is smaller, the electrical conductivity will be higher. Captopril adsorption onto $B_{16}N_{16}$-fullerene leads to a considerable decrease in E_g. Given that conductivity is proportionate to the decrement in E_g value, it can be presumed that conductivity increases when the E_g value reduces. SWBNNT and $B_{16}N_{16}$-fullerene electrical properties are very obvious after captopril molecule adsorption. As a result, not only can SWBNNT and $B_{16}N_{16}$-fullerene act as the drug delivery system for captopril, but they can also be considered as possible nanosensors or detectors for captopril. The ΔE_g values show that the interaction of captopril and SWBNNT is weaker compared to the interaction of captopril and SWCNT.

3.6. Analysis of surfaces of molecular electrostatic potential (MEP)

MEP analysis was used to investigate the distribution of charge and interpret the interaction between the captopril molecule and nanostructures (SWCNT, SWBNNT, and C_{32} and $B_{16}N_{16}$ fullerenes). The following equation defines the MEP analysis produced by molecular charge distribution [38]:

$$V(r) = \sum_A \frac{Z_A}{|R_A - r|} - \int \frac{\rho(r')dr'}{|r - r'|} \tag{3}$$

Z_A is the charge of the nucleus A, which is located at R_A. The sign of V (r) depends on whether the effects of the nucleus or electrons are dominant at a point. Based on the MEP analysis, positively charged atoms were blue, and negatively charged ones were red (Fig. 4) [39–41]. It can be predicted that the interaction of captopril with SWCNT and C_{32} fullerene will lead to charge transfer from captopril to SWCNT (Fig. 4a) and C_{32} fullerene (Fig. 4c). On the other hand, the interaction of captopril with SWBNNT and $B_{16}N_{16}$ will result in charge transfer from SWBNNT (Fig. 4b) and $B_{16}N_{16}$ (Fig. 4d) to captopril (Fig. 4b). The charge transfer between captopril and nanostructures will result in a weak interaction.

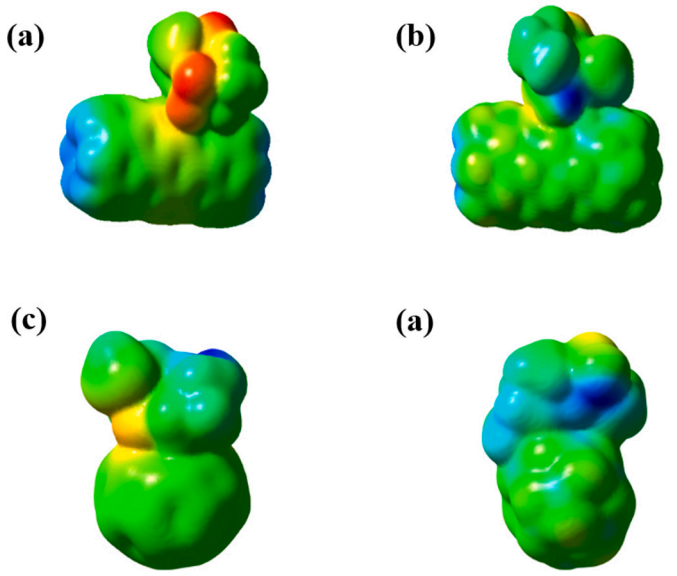

Fig. 4. Calculated molecular electrostatic potential (MEP) surfaces (a) Captopril@SWCNT, (b) Captopril@SWBNNT, (c) C_{32}-fullerene@Captopril and (d) $B_{16}N_{16}$-fullerene@Captopril.

3.7. FMO analysis

Frontier molecular orbitals, i.e., HOMO and LUMO energy surfaces, represent the ability of a molecule to donate and accept electrons, respectively. The energy gap between the HOMO and LUMO surfaces (E_g) can be utilized to determine the biological activity, chemical reactivity, and kinetic stability of a molecule [42]. The HOMO and LUMO surfaces of captopril with C_{32}-fullerene, $B_{16}N_{16}$-fullerene, SWCNT, and SWBNNT are illustrated in Fig. 5. In Captopril@C_{32}-fullerene, Captopril@SWCNT, and Captopril@SWBNNT, the HOMO and LUMO orbitals are localized over C_{32}-fullerene, SWCNT, and SWBNNT parts, respectively. In Captopril@$B_{16}N_{16}$-fullerene, the HOMO orbital is located on the captopril drug, while the LUMO orbital is situated on the $B_{16}N_{16}$-fullerene part, suggesting electron transfer from captopril to $B_{16}N_{16}$-fullerene. A compound with a low energy gap shows high chemical reactivity and less stability and vice versa [43]. The calculated E_g values for Captopril@C_{32}-fullerene, Captopril@$B_{16}N_{16}$-fullerene, Captopril@SWCNT, and Captopril@SWBNNT are obtained as 3.6346, 8.7027, 1.6174, and 6.9343 eV, respectively. These results indicate the Captopril@SWCNT system demonstrates greater chemical reactivity compared to other systems. The order of the stability and chemical reactivity for the systems is as follows: Captopril@$B_{16}N_{16}$-fullerene > Captopril@SWBNNT > Captopril@C_{32}-fullerene > Captopril@SWCNT and Captopril@SWCNT > Captopril@C_{32}-fullerene > Captopril@SWBNNT > Captopril@$B_{16}N_{16}$-fullerene.

3.8. Analysis of quantum theory of atoms in molecules (QTAIM)

According to QTAIM, electrons are distributed in the space inside the nuclei's gravitational field. The nucleus acts as an attractor in a negatively charged cloud with the charge density ($\rho(r)$). In this theory, a set of identified points is accessible as the bond critical point (BCP). They have some properties that could be used for the identification of intermolecular interactions. At critical points in these interactions, the bond type is also affected by electron density. The critical point (C_P) shows the maximum charge density. The value of $\rho(r)$ in BCP refers to the strength and degree of the bond. H_C is the electron energy density at BCP, K_C is

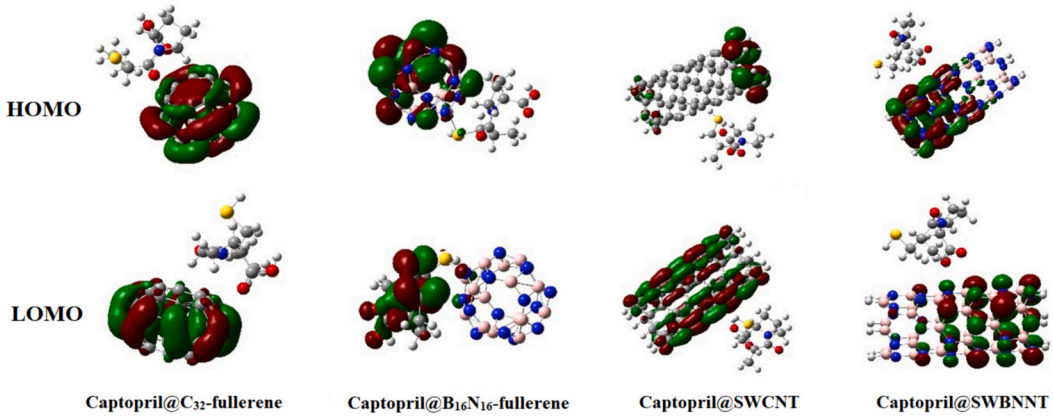

Fig. 5. FMO for the interaction of captopril with C_{32}-fullerene, $B_{16}N_{16}$-fullerene, SWCNT, and SWBNNT.

the kinetic electron energy density, and V_C is the potential electron energy density. Since K_C is positive and V_C is negative, according to Wirral's theorem, it can be concluded that the potential energy at the critical point of the bond decreases a lot and $\nabla^2\rho(r)$ becomes negative. According to Eq. (4):

$$H_C = K_C + V_C \tag{4}$$

The nature of intermolecular bonding can be evaluated using the ratio $\left|\frac{K_C}{V_C}\right|$. A value >1 indicates non-covalent bonds, while a value between 0.5 and 1 suggests partial covalent hydrogen bonds. Based on the results from Table 2, all investigated nanostructures (Captopril@SWCNT, Captopril@SWBNNT, Captopril@C_{32}-fullerene, and Captopril@$B_{16}N_{16}$-fullerene) exhibit a ratio >1, highlighting their non-covalent nature. However, the B_{34}—S_1 bond in the Captopril@$B_{16}N_{16}$-fullerene nanostructure exhibits a ratio smaller than 1, indicating a stronger electrostatic characteristic compared to other interactions. In this research, all interactions are considered weak due to the presence of $H_C > 0$. The electron density $\rho(r)$ is a crucial parameter for describing intermolecular interactions. The $\rho(r)$ values for the discussed nanostructures range from 0.00156 to 0.07444 a.u., indicating the presence of various interactions with different strengths. Consequently, the weakest interaction corresponds to N_{58}—H_{38} (ρ(r) = 0.00156 a.u.), while the strongest interaction pertains to B_{34}—S_1 ($\rho(r) = 0.07444$ a.u.).

Molecular graphs of the optimized Captopril@SWCNT, Captopril@SWBNNT, Captopril@C_{32}-fullerene, and Captopril@$B_{16}N_{16}$-fullerene complexes are represented in Fig. 6. The values of E_{ads} for Captopril@SWCNT, Captopril@SWBNNT, Captopril@C_{32}-fullerene, and Captopril@$B_{16}N_{16}$-fullerene demonstrate a weak interaction between nanostructures and inhibitors. The AIM results for Captopril@SWCNT, Captopril@SWBNNT, Captopril@C_{32}-fullerene, and Captopril@$B_{16}N_{16}$-fullerene complexes (Table 2) are consistent with the interaction trends projected by E_{ads} and MEP, confirming that SWCNT, SWBNNT, C_{32}-fullerene, and $B_{16}N_{16}$-fullerene can act as suitable drug delivery carriers for the captopril molecule.

3.9. Comparison of calculations from the 6-31G (d) basis set with the larger 6-311G (d, p) basis set

Table 3 presents calculations based on the 6-311G basis set, which demonstrate that the adsorption of captopril in all nanostructures is exothermic. Additionally, the energy of adsorption (E_{ads}) is higher in the gaseous phase compared to the aqueous phase. The order of E_{ads}, from highest to lowest, corresponds to SWCNT, SWBNNT, C_{32}, and $B_{16}N_{16}$ fullerenes, respectively, which are similar to the calculations using the 6-31G(d) basis set. It is worth noting that the increase in calculation accuracy was very insignificant.

4. Conclusions

The aim of this study was to conduct DFT calculations to investigate the potential interactions between captopril molecules and nanostructures, including SWCNT, SWBNNT, C_{32}, and $B_{16}N_{16}$ fullerenes. The results showed that all four nanostructures (SWCNT, SWBNNT, C_{32} and $B_{16}N_{16}$ fullerenes) were capable of interacting with captopril. The E_{ads}

Table 2
Topological parameters at BCP of interaction for Captopril with nanostructures (au).

Complex	BCP	V_C	K_C	H_C	$\rho(r)$	$\nabla^2\rho(r)$	$\lvert K_C/V_C\rvert$
Captopril@SWCNT	C_{46}—H_{41}	−0.00075	0.00291	0.00216	0.00508	−0.00366	3.88
	C_{61}—H_{40}	−0.00047	0.01029	0.00982	0.01505	− 0.01076	21.74
	C_{62}—C_{19}	− 0.00042	0.00157	0.00115	0.00256	− 0.00199	3.80
	C_{65}—H_{28}	− 0.00035	0.00115	0.00080	0.00185	− 0.00151	3.28
Captopril@SWBNNT	N_{59}—H_{36}	− 0.00053	0.00156	0.00103	0.00239	− 0.00209	2.94
	N_{58}—H_{38}	− 0.00038	0.00106	0.00068	0.00156	− 0.00144	2.79
	N_{49}—H_{35}	− 0.00054	0.00141	0.00087	0.00224	− 0.00196	2.61
	N_{51}—H_{39}	− 0.00051	0.00146	0.00095	0.00227	− 0.00198	2.86
	N_{51}—O_{15}	− 0.00061	0.00595	0.00534	0.00771	− 0.00657	9.75
	N_{51}—O_{16}	− 0.00071	0.00368	0.00297	0.00489	− 0.00439	5.18
Captopril@C_{32}-fullerene	C_{25}—H_{53}	−0.00050	0.001455	0.00095	0.00260	−0.00195	2.91
	C_{25}—O_{34}	−0.00094	0.00400	0.00306	0.00495	−0.00494	4.25
	C_{22}—O_{34}	−0.00089	0.00372	0.00283	0.00470	−0.00461	4.18
	C_{23}—O_{34}	−0.00095	0.00390	0.00295	0.00491	−0.00485	4.10
Captopril@$B_{16}N_{16}$_fullerene	B_{34}—S_1	+0.05121	0.03603	0.08724	0.07444	+0.01518	0.70
	N_{55}—N_5	−0.00049	0.00255	0.00206	0.00319	−0.003042	5.20
	N_{55}—H_{20}	−0.00070	0.00314	0.00244	0.00476	−0.00384	4.48
	N_{61}—H_{16}	−0.000724	0.00361	0.002886	0.00568	−0.00434	4.99

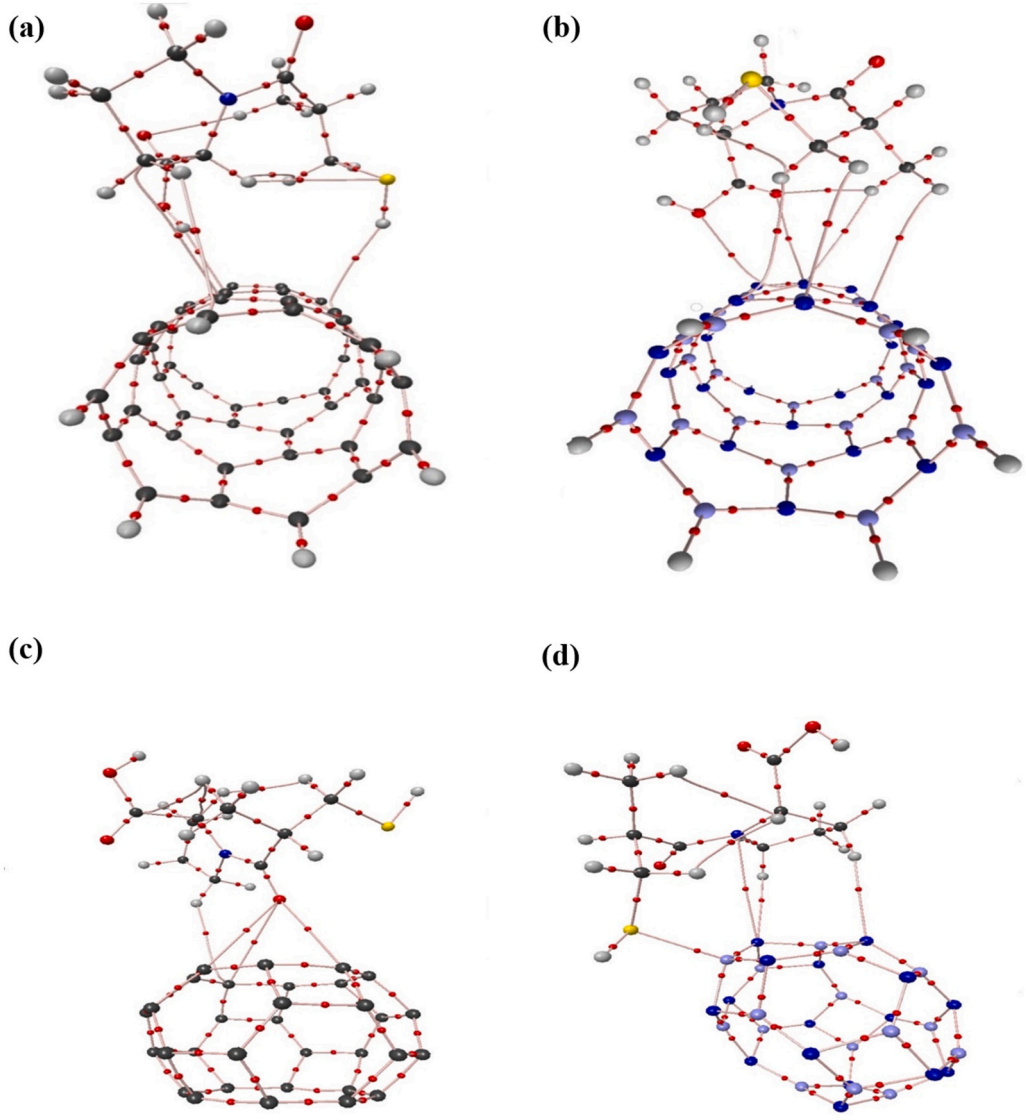

Fig. 6. Molecular graph of (a) Captopril@SWCNT complex, molecular graph of (b) Captopril@SWBNNT complex, molecular graph of (c) Captopril@C_{32}-fullerene complex, and molecular graph of (d) Captopril@$B_{16}N_{16}$ complex. Small red circles are bond critical points. The lines are bond paths. (For interpretation of the references to colour in this figure legend, the reader is referred to the web version of this article.)

Table 3
The adsorption energy (E_{ads}) of captopril onto SWCNT, SWBNNT, C_{32}, and $B_{16}N_{16}$ fullerenes in aqueous and the gaseous phases, basis set superposition error (BSSE), the HOMO-LUMO energy gaps (E_g) and the change of HOMO-LUMO gap energy upon the adsorption processes in the level of M062X/6-311G (d, p).

Nanostructures	HOMO (eV)	LUMO (eV)	E_{ads}(eV) in gas	E_{ads}(eV) in water	BSSE (eV)	E_g(eV)	ΔE_g(eV)
MWCNT	−4.2928	−2.6639	–	–	–	1.6289	–
MWBNNT	−8.3037	−1.3015	–	–	–	7.0022	–
C_{32}-fullurene	−7.2245	−3.6416	–	–	–	3.5829	–
$B_{16}N_{16}$-fullurene	−9.4368	−0.3948	–	–	–	9.0419	–
Captopril@MWCNT	−4.6748	−3.0503	−0.4128	−0.1789	0.0022	1.6245	−0.0044
Captopril@MWBNNT	−8.1987	−1.3252	−0.3722	−0.1988	0.0037	6.8732	−0.1287
Captopril@C_{32}-fullerene	−6.8400	−3.2530	−0.2905	−0.2031	0.0087	3.5870	+0.0041
Captopril@$B_{16}N_{16}$-fullerene	−8.6789	−0.1219	−0.6402	−0.6302	0.011	8.5570	−0.4849

values of captopril for SWCNT, SWBNNT, C_{32}, and $B_{16}N_{16}$ fullerenes were found to be negative in both the gaseous and aqueous phases, indicating that the adsorption of the captopril onto these nanostructures is exothermic. Additionally, the E_{ads} values revealed that the interaction between captopril and $B_{16}N_{16}$ nanocluster is stronger compared to the interactions with SWCNT, SWBNNT, and C_{32} fullerene. The ΔE_g values showed that the interaction between captopril and SWBNNT is stronger compared to the interaction between captopril and SWCNT. Specifically, the ΔE_g values for $B_{16}N_{16}$ and SWBNNT after captopril molecule adsorption were determined to be −0.4020 eV and − 0.1164 eV, respectively, indicating that the conductivity of $B_{16}N_{16}$ and SWBNNT nanostructures increased after adsorption. Therefore, $B_{16}N_{16}$ and

SWBNNT could potentially be utilized as nanosensors for captopril. Based on the analysis of the MEP, the interaction between captopril and SWCNT, as well as C_{32} fullerene, resulted in charge transfer from captopril to these nanostructures. Similarly, captopril adsorption on SWBNNT and $B_{16}N_{16}$ led to a charge transfer from $B_{16}N_{16}$ and SWBNNT to captopril. QTAIM calculations indicated a weak interaction between captopril and the nanostructures, which is consistent with the E_{ads} values. In summary, the findings suggested that all four nanostructures investigated in this study have the potential to serve as suitable drug delivery carriers for captopril. Additionally, the assessments showed that $B_{16}N_{16}$ can be used as a promising nanosensor for captopril.

CRediT authorship contribution statement

Khourshid Mehdizadeh: Writing – original draft, Validation, Data curation. **Farzad Toiserkani:** Software, Methodology, Investigation, Formal analysis. **Javad Khodabakhshi:** Software, Investigation, Formal analysis. **Narjes Hajali:** Software, Investigation, Formal analysis. **Majid Farsadrooh:** Writing – review & editing, Validation, Data curation.

Declaration of competing interest

The authors declare that they have no known competing financial interests or personal relationships that could have appeared to influence the work reported in this paper.

Data availability

Data will be made available on request.

Acknowledgments

I would like to thank the Iran Nanotechnology Initiative Council for their assistance with the collection of data.

References

[1] K.-J. Kim, M.-J. Hwang, W.-G. Shim, Y.-N. Youn, S.-D. Yoon, Sustained drug release behavior of captopril-incorporated chitosan/carboxymethyl cellulose biomaterials for antihypertensive therapy, Int. J. Biol. Macromol. 255 (2024) 128087.
[2] F. Hashemi, S. Rastegarzadeh, N. Pourreza, Response surface methodology optimized dispersive liquid–liquid microextraction coupled with surface plasmon resonance of silver nanoparticles as colorimetric probe for determination of captopril, Sensors Actuators B Chem. 256 (2018) 251–260.
[3] W. Silva Vasconcelos, G.G. da Silva, S. Alves Junior, J.V. dos Anjos, M.C. da Cunha Areias, Voltammetric determination of captopril on a glassy carbon electrode modified with copper metal-organic framework, Electroanalysis 29 (2017) 2572–2578.
[4] N. Sabbaghi, A.M. Haji Shabani, S. Dadfarnia, M. Farsadrooh, Synthesis of magnetic molecular imprinted polymer with a new functional monomer for dispersive micro solid phase extraction of captopril from wastewater and biological samples and determination by UV-Vis spectrophotometry, Microchim. Acta 190 (2023) 164.
[5] D.M. da Silva, M.C. da Cunha Areias, Rutin as an electrochemical mediator in the determination of captopril using a graphite paste electrode, Electroanalysis 32 (2020) 301–307.
[6] R.A. Soomro, M.M. Tunesi, S. Karakus, N. Kalwar, Highly sensitive electrochemical determination of captopril using CuO modified ITO electrode: the effect of in situ grown nanostructures over signal sensitivity, RSC Adv. 7 (2017) 19353–19362.
[7] M. Doust Mohammadi, H.Y. Abdullah, V. Kalamse, A. Chaudhari, Interaction of fluorouracil drug with boron nitride nanotube, Al doped boron nitride nanotube and BC_2N nanotube, Comput. Theor. Chem. 1212 (2022) 113699.
[8] M. Nouraliei, H. Javadian, K. Mehdizadeh, N. Sheibanian, A.S. Douk, F. Mohammadzadeh, N. Osouleddini, Fullerene carbon nanostructures for the delivery of phenelzine derivatives as new drugs to inhibit monoamine oxidase enzyme: molecular docking interactions and density functional theory calculations, Colloids Surf. A Physicochem. Eng. Asp. 657 (2023) 130599.
[9] M. Cao, D. Wu, M. Yoosefian, S. Sabaei, M. Jahani, Comprehensive study of the encapsulation of Lomustine anticancer drug into single walled carbon nanotubes (SWCNTs): solvent effects, molecular conformations, electronic properties and intramolecular hydrogen bond strength, J. Mol. Liq. 320 (2020) 114285.
[10] M. Aghaie, H. Aghaie, Folic acid functionalized boron nitride oxide as targeted drug delivery system for fludarabine and cytarabine anticancer drugs: a DFT study, J. Mol. Liq. 339 (2021) 116753.
[11] S. Karimzadeh, B. Safaei, T.-C. Jen, Prediction effect of ethanol molecules on doxorubicin drug delivery using single-walled carbon nanotube carrier through POPC cell membrane, J. Mol. Liq. 330 (2021) 115698.
[12] Z. Hadi, M. Nouraliei, A. Yousefi-Siavoshani, H. Javadian, S.M. Chalanchi, S. S. Hashemi, A DFT study on the therapeutic potential of carbon nanostructures as sensors and drug delivery carriers for curcumin molecule: NBO and QTAIM analyses, Colloids Surf. A Physicochem. Eng. Asp. 651 (2022) 129698.
[13] Z. Khatti, S.M. Hashemianzadeh, Boron nitride nanotube as a delivery system for platinum drugs: drug encapsulation and diffusion coefficient prediction, Eur. J. Pharm. Sci. 88 (2016) 291–297.
[14] T.H. Ferreira, D.C.F. Soares, L.M.C. Moreira, P.R.O. da Silva, R.G. dos Santos, E.M. B. de Sousa, Boron nitride nanotubes coated with organic hydrophilic agents: stability and cytocompatibility studies, Mater. Sci. Eng. C 33 (2013) 4616–4623.
[15] E. Duverger, T. Gharbi, E. Delabrousse, F. Picaud, Quantum study of boron nitride nanotubes functionalized with anticancer molecules, Phys. Chem. Chem. Phys. 16 (2014) 18425–18432.
[16] M.C. Flores Bautista, D. Cortés-Arriagada, E. Shakerzadeh, E. Chigo Anota, Acetylsalicylic acid interaction with Boron nitride nanostructures – a density functional analysis, J. Mol. Liq. 355 (2022) 118980.
[17] G. Ciofani, S. Del Turco, A. Rocca, G. De Vito, V. Cappello, M. Yamaguchi, X. Li, B. Mazzolai, G. Basta, M. Gemmi, Cytocompatibility evaluation of gum Arabic-coated ultra-pure boron nitride nanotubes on human cells, Nanomedicine 9 (2014) 773–788.
[18] M.D. Mohammadi, I.H. Salih, H.Y. Abdullah, An ultimate investigation on the adsorption of amantadine on pristine and decorated fullerenes C 5 9 X (X= Si, Ge, B, Al, Ga, N, P, and As): a DFT, NBO, and QTAIM study, J. Comput. Biophys. Chem. 20 (2021) 23–39.
[19] M. Nouraliei, M. Karimkhani, S. Mansouri, Z. Bagheri, Geometry-controlled carbon nanostructures as effective drug delivery carriers for MAO enzyme inhibitors: a DFT study, J. Mol. Liq. 340 (2021) 116857.
[20] E.B. Kalika, K.P. Katin, A.I. Kochaev, S. Kaya, M. Elik, M.M. Maslov, Fluorinated carbon and boron nitride fullerenes for drug delivery: computational study of structure and adsorption, J. Mol. Liq. 353 (2022) 118773.
[21] W.H. Moon, M.S. Son, H.J. Hwang, Theoretical study on structure of boron nitride fullerenes, Appl. Surf. Sci. 253 (2007) 7078–7081.
[22] L. Palomino-Asencio, E. García-Hernández, E. Shakerzadeh, E. Chigo-Anota, Boron-nitride nanostructures for the detection of harmful gases (CO, CO_2, H_2S, N_2O, and SO_2), Comput. Theor. Chem. 1236 (2024) 114613.
[23] H. Xu, X. Tu, G. Fan, Q. Wang, X. Wang, X. Chu, Adsorption properties study of boron nitride fullerene for the application as smart drug delivery agent of anti-cancer drug hydroxyurea by density functional theory, J. Mol. Liq. 318 (2020) 114315.
[24] F. Shojaie, A comprehensive density functional theory study on molecular structures of (5, 5) carbon nanotube doped with B, N, Al, Si, P, Co, and Ni, Comput. Theor. Chem. 1114 (2017) 55–64.
[25] J. Gong, J.W. Lam, B.Z. Tang, Benchmark and parameter tuning of hybrid functionals for fast calculation of excitation energies of AIEgens, Phys. Chem. Chem. Phys. 22 (2020) 18035–18039.
[26] D. Jacquemin, E.A. Perpete, I. Ciofini, C. Adamo, R. Valero, Y. Zhao, D.G. Truhlar, On the performances of the M06 family of density functionals for electronic excitation energies, J. Chem. Theory Comput. 6 (2010) 2071–2085.
[27] M. Walker, A.J. Harvey, A. Sen, C.E. Dessent, Performance of M06, M06-2X, and M06-HF density functionals for conformationally flexible anionic clusters: M06 functionals perform better than B3LYP for a model system with dispersion and ionic hydrogen-bonding interactions, Chem. Eur. J. 117 (2013) 12590–12600.
[28] F. Fallahpour, S.S. Gorgani, M. Nouraliei, Boron carbide nanoclusters as H_2 and N_2 gases nanosensors: theoretical investigation, Indian J. Phys. 90 (2016) 931–936.
[29] Y. Wang, P. Verma, X. Jin, D.G. Truhlar, X. He, Revised M06 density functional for main-group and transition-metal chemistry, Proc. Natl. Acad. Sci. 115 (2018) 10257–10262.
[30] S. Lakshminarayanan, V. Jeyasingh, K. Murugesan, N. Selvapalam, G. Dass, Molecular electrostatic potential (MEP) surface analysis of chemo sensors: an extra supporting hand for strength, selectivity & non-traditional interactions, J. Photochem. Photobiol. 6 (2021) 100022.
[31] M. Kurbanova, M. Ashfaq, A. Sadigova, M. Feizi-Dehnayebi, A. Maharramov, M. Tahir, A hydrazone derivative: synthesis, crystal structure, supramolecular assembly exploration by Hirshfeld surface analysis and computational study, J. Struct. Chem. 65 (2024) 92–106.
[32] Z. Akbari, C. Stagno, N. Iraci, T. Efferth, E.A. Omer, A. Piperno, M. Montazerozohori, M. Feizi-Dehnayebi, N. Micale, Biological evaluation, DFT, MEP, HOMO-LUMO analysis and ensemble docking studies of Zn(II) complexes of bidentate and tetradentate Schiff base ligands as antileukemia agents, J. Mol. Struct. 1301 (2024) 137400.
[33] R.F.W. Bader, A quantum theory of molecular structure and its applications, Chem. Rev. 91 (1991) 893–928.
[34] R.F.W. Bader, Atoms in molecules, Acc. Chem. Res. 18 (1985) 9–15.
[35] S. Melchor, J.A. Dobado, CoNTub: an algorithm for connecting two arbitrary carbon nanotubes, J. Chem. Inf. Comput. Sci. 44 (2004) 1639–1646.
[36] N.M. O'boyle, A.L. Tenderholt, K.M. Langner, Cclib: a library for package-independent computational chemistry algorithms, J. Comput. Chem. 29 (2008) 839–845.
[37] S. Nikolova, M. Milusheva, V. Gledacheva, M. Feizi-Dehnayebi, L. Kaynarova, D. Georgieva, V. Delchev, I. Stefanova, Y. Tumbarski, R. Mihaylova, Drug-delivery silver nanoparticles: a new perspective for phenindione as an anticoagulant, Biomedicines 11 (2023) 2201.

[38] S. Cox, D. Williams, Representation of the molecular electrostatic potential by a net atomic charge model, J. Comput. Chem. 2 (1981) 304–323.
[39] S. Zinatloo-Ajabshir, S. Rakhshani, Z. Mehrabadi, M. Farsadrooh, M. Feizi-Dehnayebi, S. Rakhshani, M. Dušek, V. Eigner, S. Rtimi, T.M. Aminabhavi, Novel rod-like $[Cu(phen)_2(OAc)]\cdot PF_6$ complex for high-performance visible-light-driven photocatalytic degradation of hazardous organic dyes: DFT approach, Hirshfeld and fingerprint plot analysis, J. Environ. Manag. 350 (2024) 119545.
[40] M. Milusheva, M. Todorova, V. Gledacheva, I. Stefanova, M. Feizi-Dehnayebi, M. Pencheva, P. Nedialkov, Y. Tumbarski, V. Yanakieva, S. Tsoneva, Novel anthranilic acid hybrids—an alternative weapon against inflammatory diseases, Pharmaceuticals 16 (2023) 1660.
[41] A. Rossi, C. Stagno, A. Piperno, N. Iraci, S. Panseri, M. Montesi, M. Feizi-Dehnayebi, G. Bassi, M.L. Di Pietro, N. Micale, Anticancer activity and morphological analysis of Pt(II) complexes: their DFT approach, docking simulation, and ADME-Tox profiling. Appl. Organomet. Chem., e7403.
[42] M. Milusheva, V. Gledacheva, I. Stefanova, M. Feizi-Dehnayebi, R. Mihaylova, P. Nedialkov, E. Cherneva, Y. Tumbarski, S. Tsoneva, M. Todorova, Synthesis, molecular docking, and biological evaluation of novel anthranilic acid hybrid and its diamides as antispasmodics, Int. J. Mol. Sci. 24 (2023) 13855.
[43] M.N. Tahir, K.S. Munawar, M. Feizi-Dehnayebi, M. Ashfaq, M.E. Muhammed, One-dimensional polymer of copper with salicylic acid and pyridine linkers: synthesis, characterizations, solid state assembly investigation by hirshfeld surface analysis, and computational studies, J. Mol. Struct. 1297 (2024) 136956.